Serial ^{13}C-Based Flux Analysis of an L-Phenylalanine-Producing *E. coli* Strain Using the Sensor Reactor

Aljoscha Wahl,[†,‡] Mohamed El Massaoudi,[†] Dick Schipper,[§] Wolfgang Wiechert,[‡] and Ralf Takors*[,†]

Institute of Biotechnology, Forschungszentrum Jülich GmbH, 52425 Jülich, Germany, Department of Simulation, Institute of Systems Engineering, FB 11/12, University of Siegen, Paul-Bonatz-Str. 9-11, 7068 Siegen, Germany, and DSM, P.O. Box 1, 624-0305, 2600 MA Delft, The Netherlands

With the aid of the recently developed Sensor reactor system, a series of three subsequent ^{13}C labeling experiments was performed mirroring the L-phenylalanine (L-Phe) production phase of a recombinant *E. coli* strain that was cultivated under industry-like conditions in a 300 L bioreactor. On the basis of the data from NMR labeling analysis, three subsequent flux patterns were successfully derived monitoring the L-Phe formation during an observation window from 14 to 23.3 h process time. Linear programming was performed to identify optimal flux patterns for L-Phe formation. Additionally, flux sensitivity analysis was used to identify the most promising metabolic engineering target. As a result, high rates of phosphoenolpyruvate (PEP) to pyruvate (PYR) conversion were identified as the most important reason for deterioration of the L-Phe/glucose yield from 20 to finally 11 mol %. Considering the characteristics of the enzyme kinetics involved, the working hypothesis was formulated that phosphoenolpyruvate synthase activity was increasingly hampered by rising oxaloacetate and 2-oxoglutarate concentrations, while at the same time pyruvate kinase activity arose due to activation by fructose 1,6-diphosphate. Hence, *pps* overexpression should be performed to optimize the existing production strain.

Introduction

The production of aromatic amino acids, corresponding pathway intermediates, or derivatives thereof is without doubt of great commercial importance (Frost and Lievense, 1994; Bongaerts et al., 2001; Schmid et al., 2001; Bongaerts et al., 2001; Drauz et al., 2002). Several production approaches have been published using, for instance, recombinant *E. coli* strains. Examples are the production of pathway intermediates such as 3-dehydroshikimic acid (Li et al., 1999), shikimic acid (Chandram et al., 2003), chorismate derivatives such as *trans*-2,3-cyclohexanediole (Franke et al., 2003a), or *trans*-3,4-cyclohexanediole (Franke et al., 2003b) and the final pathway products L-tryptophane, L-tyrosine, and L-phenylalanine (Bongaerts et al., 2001; Drauz et al., 2002; Gerigk et al., 2002). Among these products, L-phenylalanine currently represents the largest economical market with 11 000 to 12 000 tons per year and a product price of 20−40 US$/kg depending on the product purity (Bongaerts et al., 2001). In the case of L-phenylalanine, the majority is used for the production of the artificial sweetener aspartame, for instance, in the "Thermolysine" process at DSM, The Netherlands (Schmid et al., 2001).

Motivated by these promising commercial perspectives, several studies were previously performed investigating the optimum supply for the pathway precursors D-erythrose-4-phosphate (E4P) and phosphoenolpyruvate (PEP). To ensure a sufficient E4P availability, transaldolase (*tal*) (Lu and Liao, 1997) and/or transketolase (*tktA*) overexpression was studied (Draths et al., 1992) and subsequently combined with phosphoenolpyruvate synthase (*pps*) overexpression (Patnaik and Liao, 1994; Patnaik et al., 1995; Berry, 1996; Gosset et al., 1996; Yi et al., 2002; Chandram et al., 2003) or alternative glucose uptake systems in phosphotransferase system (*pts*)-negative strains (Berry, 1996; Gosset et al., 1996; Flores et al., 1996; Chen et al., 1997). In addition, Csr (carbon storage regulator) disrupted strains were used to ensure a sufficient PEP supply (Tatarko and Romeo, 2001).

Despite the invaluable importance of these results for the optimization of the aromatic amino acid precursor supply, detailed (^{13}C-based) flux analysis has not yet been used to elucidate intracellular flux redistributions in strains producing aromatic amino acid pathway intermediates or final products such as L-phenylalanine. So far, flux analysis has been applied to estimate (theoretical) optimum flux distributions in DAHP (3-desoxy-arabino-heptulosonate-7-phosphate)-producing strains (Patnaik and Liao, 1994; Patnaik et al., 1995), which even achieved a glucose-to-DAHP conversion with theoretical yield (Liao et al., 1996). Also, the effect of pts inactivation for DAHP production was studied (Flores et al., 2002). However, one should consider that metabolic flux analysis for L-phenylalanine producers significantly differs from the DAHP studies because of the second PEP molecule needed for L-phenylalanine biosynthesis. It is also noteworthy that all studies were limited to shake flasks or small, lab-scale bioreactors that obviously did not represent industry-like production conditions in large-scale bioreactors.

* Corresponding author. Phone: +49/2461/613365. Fax: +49/2461/613870. E-mail: r.takors@fz-juelich.de.
[†] Institute of Biotechnology.
[‡] University of Siegen.
[§] DSM.

10.1021/bp0342755 CCC: $27.50
Published on Web 03/11/2004

Hence it is the aim of this study to apply detailed ^{13}C-based metabolic flux analysis to an L-phenylalanine (L-Phe)-producing *E. coli* strain. With the aid of a recently developed Sensor reactor (El Massaoudi et al., 2003; Drysch et al., 2003a; Drysch et al., 2003b), carbon flux distributions in the L-Phe producing *E. coli* 4pF81 strain were studied under realistic, 300 L-scale production conditions, described elsewhere (Gerigk et al. 2002, Rüffer et al., 2003). A series of carbon flux maps will be presented on the basis of ^{13}C labeling experiments, identifying changing intracellular flux distributions during the L-phenylalanine production phase. The series of flux maps is compared to the theoretical, optimum flux distribution. Additionally, a flux sensitivity analysis is presented and a working hypothesis for further production strain optimization is derived.

Material and Methods

Strain and Cultivation Conditions. The L-Phe production strain *E. coli* 4pF81, presented elsewhere (Rüffer et al., 2003) based on *E. coli* K 12 LJ110 (Zeppenfeld et al., 2000) was used. The genotype was *E. coli* LJ110 Δ(*pheA tyrA aroF*) pJF119EH *aroF pheA*^{fbr} *aroB aroL*. The genes *pheA* (encodes chorismate mutase/prephenate dehydratase), *tyrA* (encodes chorismate mutase/prephenate dehydrogenase), and *aroF* (encodes tyrosine feedback-inhibited DAHP synthase) were deleted in the chromosome. The strain was tyrosine auxotrophic to prevent carbon flux into tyrosine synthesis. The plasmid pJF119EH carried the genes *aroF*, *pheA*^{fbr} (resistant against feedback inhibition by L-phenylalanine), *aroB* (encodes 3-dehydroquinate synthase), and *aroL* (encodes shikimate kinase II). This plasmid-encoded gene overexpression was performed to avoid an unwanted accumulation of pathway intermediates upstream of the enzymes encoded by the above-mentioned genes. The genes were under control of the IPTG-inducible P_{tac} promoter. Ampicillin resistance was plasmid encoded as a selection marker for plasmid-containing cells.

For shaking flask cultivations, the following medium was used: 0.3 g/L $MgSO_4 \cdot 7H_2O$, 0.015 g/L $CaCl_2 \cdot 2H_2O$, 3.0 g/L KH_2PO_4, 12 g/L K_2HPO_4, 0.1 g/L NaCl, 5.0 g/L $(NH_4)_2SO_4$, 0.075 g/L $Fe(SO_4)_2 \cdot 7H_2O$, 1.0 g/L Na−citrate, 1.5 mL/L trace element solution, 0.0075 g/L vitamin B1 (thiamine HCl), 0.08 g/L tyrosine, 5.0 g/L glucose$\cdot H_2O$, 0.1 g/L ampicillin. The trace element solution consisted of: 2.0 g/L $Al_2(SO_4)3 \cdot 18H_2O$, 0.75 g/L $CoSO_4 \cdot 7H_2O$, 2.5 g/L $CuSO_4 \cdot 5H_2O$, 0.5 g/L H_3BO_4, 24 g/L $MnSO_4$, 3.0 g/L $Na_2MoO_4 \cdot 2H_2O$, 2.5 g/L $NiSO_4 \cdot 6H_2O$, 15 g/L $ZnSO_4 \cdot 7H_2O$.

Four shaking flasks with 250 mL of culture were used to inoculate the 30 L bioreactor. The preculture medium of the 30 L bioreactor was the same as the shaking flask medium. *E. coli* was cultivated at pH 6.5 and 37 °C with 0.5 bar overpressure (aeration rate: 1 vvm). The dissolved oxygen level was controlled at 30%, ensuring aerobic conditions. After $OD_{620} \sim 3$ was reached in the 30 L bioreactor, a liquid volume of 11 L was pumped into the 300 L bioreactor. Here, the same medium was used as before except for higher concentrations of $Fe(SO_4)_2 \cdot 7H_2O$ (0.1125 g/L), Na−citrate (1.5 g/L), glucose$\cdot H_2O$ (15.0 g/L), and trace element solution (1.5 mL/L).

When *E. coli* 4pF81 was cultivated in the 300 L fed-batch process, a tyrosine-containing feed (20 mL/min, 25 g/L, dissolved in 5% NH_3 to increase its solubility) was started at the beginning of the exponential growth phase ($OD_{620} \sim 8$) lasting until OD ~ 80 was reached. After this, the feed was drastically reduced to 1 mL/min until the end of the fermentation to fulfill only maintenance demands of the cells. The glucose feed profile (containing 600 g/L glucose$\cdot H_2O$) was based on previous experiments published elsewhere (Rüffer et al., 2003) and was manually controlled such that no significant glucose accumulation occurred in the production process. All feed profiles of the Sensor reactor were similar to the production process but automatically scaled down (with the aid of LabView process control) with respect to the current liquid volume ratio of the two processes. In addition a reduced tyrosine concentration of 2.5 g/L was used in the Sensor reactor feed to allow an accurate feeding. After OD_{620} 10−15 was achieved, 100 μM IPTG was added for induction. Fermentation details can be found elsewhere (Gerigk et al., 2002).

Sensor Reactor System. The 1 L Sensor reactor (controlling device: Infors, Basel, Switzerland) was installed close to the 300 L production reactor (Chemap, Volketswil, Switzerland) and connected to the production process in master/slave mode. Moving averages of five on-line measurements of dissolved oxygen (DO), pH, temperature, pressure, and aeration of the production reactor were used as set points for the Sensor reactor via a LabView (National Instruments Corporation, Austin, TX)-based process control system (for details, see El Massaoudi et al., 2003). pH control was realized by addition of 10% NH_4OH.

At the beginning of each labeling period, a well-defined inoculation sample of 1 L was automatically taken out of the production process via a special inoculation unit. Subsequently, 1-^{13}C-labeled glucose was pulsed into the Sensor reactor, and the scaled-down feeding profile, containing 1-^{13}C glucose, was started (for labeling details, see below). The Sensor reactor ran in parallel to the production process for 2.5 to 3 h, thus ensuring a sufficient labeling pattern in the supernatant. After one labeling period was finished, the Sensor reactor was completely emptied, cleaned via over-pressurized aeration and steam streaming (for details see El Massaoudi et al., 2003), and prepared for the next labeling experiment monitoring a subsequent phase of the production process. In general, the experimental carbon balance was closed at about 92%.

Labeling and Sampling. Immediately before each labeling experiment, the current glucose concentration of the production process was measured and the liquid volume containing 140 g/L of [1-^{13}C] glucose (99% atom enrichment, Cambridge Isotope Laboratories, Andover, MA) was calculated and subsequently pulsed into the Sensor reactor (with the aid of an automatic pulsing device, El Massaoudi et al., 2003) to ensure a 25% content of labeled glucose. Then, the scaled-down (see above) glucose feed of the Sensor reactor was started, containing the same fraction (25%) of labeled glucose. Following this procedure, the ^{13}C enrichment was kept constant at 25% throughout the entire labeling period (see also Table 1). Samples were taken in 20 min intervals from the Sensor reactor and from the production process. The samples were centrifuged, and the supernatant was stored at −20 °C for subsequent HPLC and NMR analysis.

Sample and Labeling Analysis. Glucose was measured by using an enzymatic analysis kit (Boehringer, Mannheim, Germany) with hexokinase (EC 2.7.1.1.) and glucose-6-phosphate-dehydrogenase (EC 1.1.1.49). Biomass dry weight was determined gravimetrically and showed a linear relationship with photometric turbidity measurements at 620 nm. Amino acids were analyzed by HPLC after derivatization with *ortho*-phthaldialde-

Table 1. Flux Estimations of the ^{13}C-Based Flux Analysis[a]

	experiment A, 14−16.8 h		experiment B, 17.2−20 h		experiment C, 20.5−23.3 h	
reaction	flux [mM/h]	error [mM/h]	flux [mM/h]	error [mM/h]	flux [mM/h]	error [mM/h]
upt1	17.52	0.30	14.13	0.30	13.43	0.30
upt2	52.08	0.30	42.31	0.30	39.47	0.30
emp1	31.79	8.50	34.62	8.98	49.90	26.27
emp2	52.29	2.85	45.60	3.01	49.90	8.76
emp3	52.29	2.85	45.60	3.01	49.90	8.76
emp4	197.77	2.94	91.36	3.09	96.81	8.79
ppp1	37.81	8.51	21.82	8.99	3.00	26.27
ppp2	20.50	5.67	10.99	5.99	0.00	17.51
ppp3	17.31	2.84	10.84	3.00	3.00	8.76
ppp4	3.19	2.84	0.15	3.00	−3.00	8.76
ppp5	17.31	2.84	10.84	3.00	3.00	8.76
ppp6	17.31	2.84	10.84	3.00	3.00	8.76
tcc	79.27	3.00	69.65	3.15	84.63	8.81
ana1	0.26	0.02	0.33	0.02	0.2	0.02
ura	0.26	0.02	0.33	0.02	0.2	0.02
dahp shi phe	14.12	0.20	10.69	0.20	5.99	0.2
CO_2 *aux*	289.50	3.11	241.14	3.09	262.67	3.09

[a] Because the labeling patterns in PEP and PYR could not be distinguished, a common PEP/PYR pool was used for modeling. The flux *emp5* shown in Figure 2 is not included in the ^{13}C model; it can only be identified later by stoichiometric constraints. The reactions and atom transitions are shown in Table 5. *upt1* and *upt2* code for the uptake of labeled and nonlabeled glucose, respectively, allowing the conclusion that the prechosen aim of 25% ^{13}C enrichment was well achieved.

Table 2. Stoichiometric Matrix Used for Linear Programming[a]

metabolite	reactions																		
constraints	*pts*	*emp1*	*emp2*	*emp3*	*emp4*	*emp5*	*ppp1*	*ppp2*	*ppp3*	*ppp4*	*ppp5*	*ppp6*	*tca*	*dahp*	*shi*	*phe*	*resp*	*fut*	*thy*
G6P	1	−1	0	0	0	0	−1	0	0	0	0	0	0	0	0	0	0	0	0
F6P	0	1	−1	0	0	0	0	0	0	1	0	1	0	0	0	0	0	0	0
FBP	0	0	1	−1	0	0	0	0	0	0	0	0	0	0	0	0	0	0	0
GAP	0	0	0	2	−1	0	0	0	0	1	1	−1	0	0	0	0	0	0	0
PEP	−1	0	0	0	1	−1	0	0	0	0	0	0	0	−1	0	−1	0	0	0
PYR	1	0	0	0	0	1	0	0	0	0	0	0	−1	0	0	0	0	0	0
Ru5P	0	0	0	0	0	0	1	−1	−1	0	0	0	0	0	0	0	0	0	0
X5P	0	0	0	0	0	0	0	1	0	−1	−1	0	0	0	0	0	0	0	0
Ri5P	0	0	0	0	0	0	0	0	1	0	−1	0	0	0	0	0	0	0	0
E4P	0	0	0	0	0	0	0	0	0	−1	0	1	0	−1	0	0	0	0	0
S7P	0	0	0	0	0	0	0	0	0	0	1	−1	0	0	0	0	0	0	0
DAHP	0	0	0	0	0	0	0	0	0	0	0	0	0	1	−1	0	0	0	0
SHI	0	0	0	0	0	0	0	0	0	0	0	0	0	0	1	−1	0	0	0
NADH	0	0	0	0	1	0	0	0	0	0	0	0	3	0	0	0	−1	0	−1
NADPH	0	0	0	0	0	0	2	0	0	0	0	0	0	0	−1	0	0	0	1
ATP	0	0	−1	0	1	1	0	0	0	0	0	0	0	0	0	−1	1,8	−1	0
Upt=1	1	0	0	0	0	0	0	0	0	0	0	0	0	0	0	0	0	0	0

[a] Linear programming approach is based on the assumption of a constant P/O ratio (constant NADH/ATP conversion *resp* at 1.8). Balances for cometabolites NADPH, NADH, and ATP are "open". Ample ATP can be consumed by the futile reaction *fut*. Reactions of the tricarboxylic cycle were lumped to *tca*, which is motivated by the lacking efflux rates into the amino acid synthesis during L-Phe production with tyrosine-limited, nongrowing cells. It is noteworthy that the stoichiometric model possesses two degrees of freedom, which are fulfilled by the maximization constraints optimum L-Phe flux and minimum futile cycle activity.

hyde (OPA), separation on a reverse-phase column, and detection of the fluorescence of the OPA derivative (Ogden and Földi, 1992). Organic acids were measured by using an Aminex HPX-87H column (Biorad, Munich, Germany) eluted at 40 °C with 0.2 N H_2SO_4. The UV absorption was detected at 254 nm.

^{13}C NMR spectra (with proton decoupling) were recorded at 90.56 MHz in 5 mm tubes on a Bruker AMX 360. Prior to measurements, samples were lyophilized and redissolved in D_2O at twice the original concentration. A small amount of EDTA was added (5 mg/mL) to chelate the metal ions. To eliminate NOEs and ensure quantitative results, the decoupler was switched off during the 45 s recycling delay (5 times the longest T_1). Acquisition parameters: spectral width 240 ppm; pulse width 6 μs (90° flip angle); data size 80K; acquisition time 1.88 s; number of scans 4800. A line broadening of 1 Hz was applied, and 128K data were used for the processed spectra. The enrichments were calculated from the integrals of the individual carbon atoms, where positions 2, 4, and 6 + 8 gave identical integral values and were assumed to not be enriched.

Modeling and Sensitivity Analysis. For calculation of the intracellular fluxes, it was assumed that the Sensor reactor was in a quasisteady state, i.e., the intra- and extracellular fluxes were constant over the timespan of the labeling experiment leading to equilibrated labeling patterns in the metabolite pools. The measured ^{13}C enrichments of the supernatant pools had to be corrected due to the dilution by nonlabeled metabolites that were produced before the labeling experiment (see Table 4). The enrichment (x) [%] achieved during the labeling period was calculated from the ^1H NMR measurements (y) [%] with the molar fraction (p) [mol/mol %] of produced phenylalanine following the eq 1:

$$y = px + (1 - p)0.011 \quad (1)$$

Extracellular fluxes such as glucose uptake, product formation, and CO_2 production were calculated from concentration measurements and corrected for dilution

Table 3. Measured Extracellular Fluxes Used for Metabolic Flux Analysis[a]

	fluxes [mmol/Lh]				
	upt1	*upt2*	L-Phe	CO_2	uracil
phase A	17.53	52.09	14.12	253.6	0.26
phase B	14.13	42.32	10.69	238.1	0.33
phase C	13.48	39.52	5.96	209.2	0.2

[a] *upt1* and *upt2* indicate the 1-^{13}C-labeled and the nonlabeled glucose uptake.

Table 4. Label Enrichments at Certain C-Positions of L-Phe[a]

	raw data			corrected data	
	C3 [%]	C5 + C9 [%]	*p* [%]	C3 [%]	C5 + C9 [%]
phase A	4.50	3.90	39.26	9.76	8.23
phase B	3.80	3.10	23.66	12.51	9.55
phase C	3.20	2.60	11.83	18.86	13.78

[a] Corrections due to signal dilution are included. *p* represents the fraction of L-Phe produced during the labeling experiment compared to the total amount found in the supernatant. The corrected values were used for ^{13}C-based flux estimation.

due to glucose feeding and sampling (see Table 4). ^{13}C flux estimation was carried out using the software 13C FLUX (Möllney et al., 1999; Wiechert et al., 1999). The metabolic model included reactions from glycolysis, pentose phosphate pathway and the tricarboxylic acid cycle (see Table 5). The glyoxylic shunt was assumed to be inactive under the aerobic experimental conditions. According to Fischer and Sauer (2003) and Peekhaus and Conway (1998), the Entner−Doudoroff (ED) pathway only plays a minor role in (wild-type) *E. coli* central metabolism and therefore was neglected in the model. The pools PEP and PYR as well as oxalacetate and malate were lumped, leading to a *pts* decoupling from the PEP/PYR conversion. The reactions of the L-Phe production pathway and the respective C-atom transitions are also shown in Table 5. Fluxes were estimated by using an evolutionary optimization, which was followed by a local optimization (optimizers are CooolEvoAlpha and CooolBFGSAlpha from the Coool library, http://coool.mines.edu/).

Linear Programming. A stoichiometric approach can be used to determine the theoretical, optimal flux distribution for maximum phenylalanine production. It was assumed that no growth occurred during the production phase, i.e., there were no fluxes into the biomass. The model included metabolites of the glycolysis (G6P, FBP, PEP, PYR), pentose-phosphate (Ru5P, RiP, S7P, E4P), and aromatic amino acid (DAHP, SHI) pathways. Metabolites of the tricarboxylic acid cycle were not balanced but lumped into one reaction step. Co-Metabolites such as NADH, NADPH, and ATP were included with "open" balances; for instance futile cycling (*fut*) was allowed as a free flux to consume ample ATP. It was assumed that the L-Phe-producing strain possessed an active PEP synthase (Pps, represented by reaction *emp5*) and a transhydrogenase (thy) reaction enabling the proton transfer from NADH to NADPH. In total, the model consisted of 16 balanced metabolites and 19 reactions (Table 1) signifying three degrees of freedom. To cover three degrees, the input flux (*pts*) was set to one, the production flux was maximized, and futile cycling (*fut*) was minimized. Furthermore, some flux limits were given such as respiration, TCA, and futile cycling had to be positive (*resp*, *tca*, *fut* $\geq$ 0).

Sensitivity Analysis. To qualify the sensitivity of the flux distributions, a linear programming approach was followed. The basic idea was to derive flux sensitivity data that were not as dependent on the choice of free fluxes as in the classical approach of Delgado and Liao (1997). Based on the experimentally determined metabolic fluxes, the glucose uptake was set constant together with one of the interesting fluxes such as *emp5, ppp1*, *ppp4*, or *ppp6*. Use of the constraint of L-Phe flux

Table 5. Model Reactions and Atom Transitions for ^{13}C Flux Analysis[a]

name	reaction	C-atom transition
upt1	Gluc13C > G6P	#ABCDEF > #ABCDEF
upt2	GlucNat > G6P	#ABCDEF > #ABCDEF
emp1	G6P > F6P	#ABCDEF > #ABCDEF
emp2	F6P > FBP	#ABCDEF > #ABCDEF
emp3	FBP > GAP + GAP	#ABCDEF > #CBA + #DEF
emp4	GAP > PEP/PYR	#ABC > #ABC
ppp1	G6P > CO2 + Ru5P	#ABCDEF > #A + #BCDEF
ppp2	Ru5P > x5P	#ABCDE > #ABCDE
ppp3	Ru5P > Ri5P	#ABCDE > #ABCDE
ppp4	X5P + E4P > GAP + F6P	#ABCDE + #abcd > #CDE + #ABabcd
ppp5	X5P + Ri5P > S7P + GAP	#ABCDE + #abcde > #ABabcde + #CDE
ppp6	GAP + S7P > E4P + F6P	#ABC + #abcdefg > #defg + #abcABC
tcc1	PEP/Pyr > AcCoA + CO2	#ABC > #BC + #A
tcc2	AcCoA + MAL/OAA > ICIT	#AB + #abcd > #dcbaBA
tcc3	ICIT > AKG + CO2	#ABCDEF > #ABCEF + #D
tcc4	AKG > SUC + CO2	#ABCDE > #BCDE + #A
tcc5a	SUC > MAL/OAA	#ABCD > #ABCD
tcc5b	SUC > MAL/OAA	#ABCD > #DCBA
ana1	PEP/PYR + CO2 > MAL/OAA	#ABC + #a > #ABCa
ura	MAL/OAA + CO2 > Uracil + CO2	#ABCD + #a > #CBAa + #D
Uracilaux	Uracil > UracilAux	#abcd > #abcd
dahp	PEP/PYR + E4P > DAHP	#ABC + #abcd > #ABCabcd
shi	DAHP > SHI	#ABCDEFG > #BCDEFGA
pheA	PEP/PYR + SHI > L-Phe + CO2	#ABC + #abcdefg > #ABCabcdef + #g
pheB	PEP/PYR + SHI > L-Phe + CO2	#ABC + #abcdefg > #ABCafedcb + #g
Pheaux	PHE > PHEAux	#ABCEFGHIJ > #ABCEFGHIJ
CO2aux	CO2 > CO2Aux	#A > #A

[a] *upt1* and *upt2* indicate the 1-^{13}C-labeled and the nonlabeled glucose uptake. It is noteworthy that *pheA* and *pheB* code for the same synthesis step with different atom transitions because the orientation of the L-Phe ring can be mirrored. It is assumed that the two orientations appear equally. C-atom transitions are indicated by letter sequences and represent the basis for the setup of the isotopomer transition matrix.

maximization allowed the rest of the metabolic network to rearrange. Basically, the resulting flux patterns thus represent optimum L-Phe formation rates under the constraint that each of the subsequently fixed fluxes *emp5*, *ppp1*, *ppp4*, or *ppp6* could not be amplified because of biochemical limitations or gene regulations. High L-Phe formation rates thus indicate that the corresponding fixed flux does not significantly hamper the reachable, optimal L-Phe yield. On the other hand, the lowest achievable L-Phe yield obviously corresponds to the limiting affect of the fixed flux, thus revealing it as a promising metabolic engineering target.

Results and Discussion

As expressed above, the study followed the idea of analyzing changing carbon flux patterns under realistic (300 L bioreactor) production conditions making use of the recently presented Sensor reactor approach (El Massaoudi et al., 2003). The following questions guided the study:

Were real, intracellular flux distributions optimal with respect to maximum L-Phe formation? If not, where were the main discrepancies and how significant were they?

Did the flux patterns change during the production period? If so, what were the main reasons?

Because previous experiments (Rüffer et al., 2003) revealed maximum product formation rates shortly after the beginning of the tyrosine-limited production phase (followed by a significant product formation decline), this period was chosen to study changing intracellular flux maps and to derive thereupon working hypotheses including promising metabolic engineering targets for further production strain improvement.

As indicated in Figure 1, labeling periods were realized from 14 to 16.8 h, 17.2 to 20 h, and 20.5 to 23.3 h of process time. Before, biomass production stopped at $OD_{620} \sim 80$ (after 11 h) as a result of the significantly reduced tyrosine feed as described above. Because [1-^{13}C] glucose was pulsed into the Sensor reactor to achieve 25% ^{13}C glucose enrichment in the supernatant, the total glucose level in the Sensor reactor was accordingly higher compared to the production process following the same course, especially during phases B and C. Differences between the glucose curves occurred during phase A, because glucose feeding into the Sensor reactor was too high due to erroneous liquid volume measurements. However, different cultivation conditions did not result because glucose levels of both reactors ensured well-saturated glucose uptake (Ferenci et al., 1996). Moreover, the ^{13}C enrichment in the Sensor reactor was not affected because the post-pulse ^{13}C glucose fraction in the supernatant was the same as in the feed.

With respect to the measured metabolite concentration courses in the supernatant, a high degree of similarity was found. The L-Phe accumulation was almost identical in both reactors (regression coefficient $r = 0.999$). This holds also true for the uracil synthesis ($r = 0.971$) following the β-alanine route via aspartate and oxaloacetate, respectively. Obviously, the two intermediates of the aromatic amino acid pathway, 3-dehydroshikimate (DHS) and shikimate (SHI), were produced before Sensor reactor monitoring was started. Their production stopped during the labeling periods, which was indicated by an almost constant level.

In the case of the oxygen uptake rate (OUR), high degrees of similarity were found regarding the Sensor and the production reactor. The dissolved oxygen concentration (DO) was always above 30% in both processes

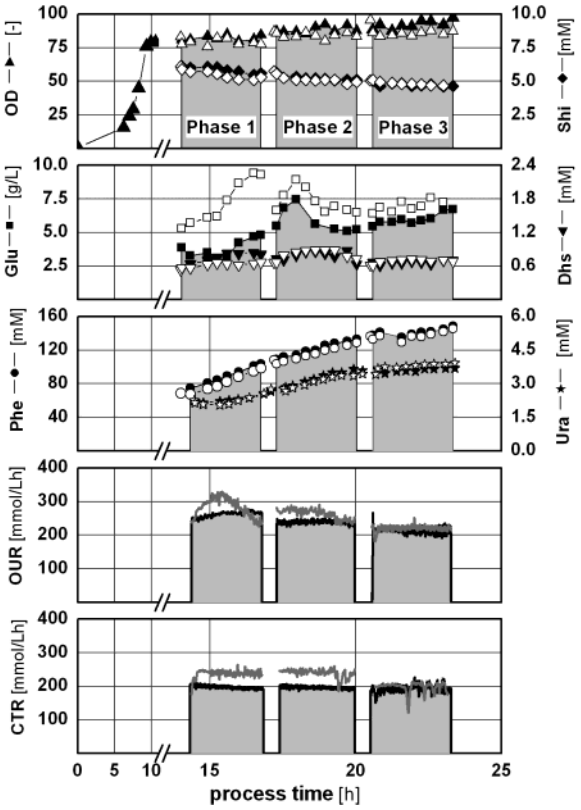

Figure 1. Comparison of phenomenological state variables such as optical density (OD_{620}), glucose concentration, L-phenylalanine concentration (L-Phe), and the oxygen uptake rate (OUR) together with the carbon dioxide transfer rate (CTR). All variables are shown for the production process (black symbols/lines) and for the Sensor reactor (hollow symbols/grey lines). Labeling experiments were started after 14, 17.2, and 20.5 h lasting for approximately 2.5 h each.

(data not shown), thus ensuring a nonlimited oxygen supply. On the other hand, carbon dioxide transfer rates (CTR) in the Sensor reactor were observed to be 15−20% higher than in the production process during phases A and B. However, this is an "artificial" offset that occurred as a consequence of the maximum CO_2 detection limit that was reached in the exhaust gas analysis device used to monitor the production process.

In summary, we have concluded that the phenomenology of both processes was sufficiently consistent, thus allowing both ^{13}C-based flux analysis for the three labeling phases and transfer of the results from the 1 L Sensor reactor to the 300 L-scale production process.

Results of the detailed flux analysis are given in Figure 2, showing standardized fluxes (mol %) with respect to the glucose uptake rate. Additionally, Table 1 contains the absolute flux values (mmol L^{-1} h^{-1}) with the corresponding errors. As shown, most of the fluxes were estimated with sufficient accuracy within error margins of 5−15%, especially for the flux estimations of phases A and B. High deviations (>25%) were found for the reactions *emp1* (glucose 6-phosphate isomerase), *ppp1* (oxidative pentose phosphate pathway), and *ppp2* (ribulose-5-phosphate epimerase), respectively. Most presumably, these deviations were caused by a lack of nucleoside labeling information (e.g., from RNA or DNA) considering ribose-5-phosphate (Ri5P) as the precursor, which was not accessible using strains under nongrowing L-Phe production conditions. This lack of additional information becomes apparent for the flux estimates of *emp1*, *ppp1*, and *ppp2* in phase C. These fluxes were no longer

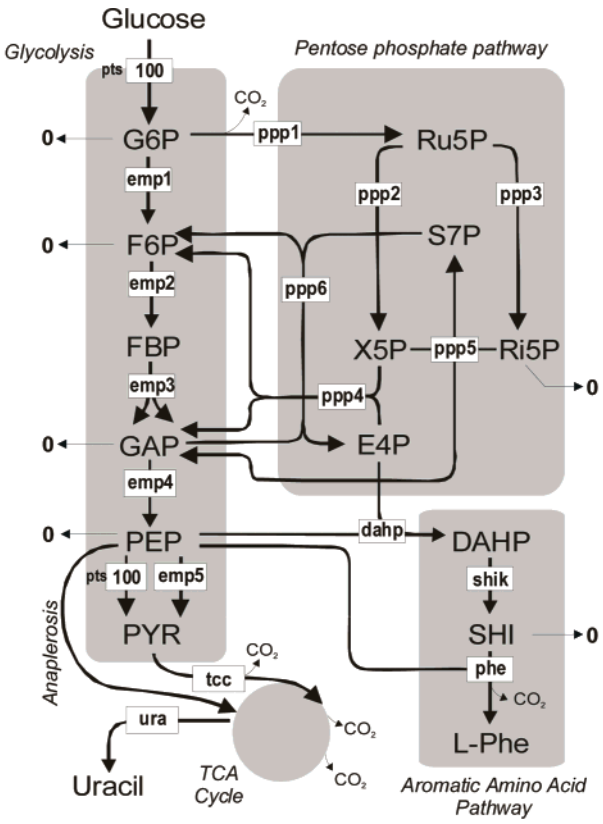

	Glycolysis				Pentose phosphate pathway					TCA	Products		
	emp1	emp2 emp3	emp4	emp5	ppp1	ppp2	ppp3	ppp4	ppp5 ppp6	tcc	CO2 aux	Ura	dahp shik phe
Opt	97	79	119	-100	3	-18	21	-39	21	0	63	0	60
A (14-16.8)	46	75	155	14	54	29	25	5	25	114	416	0.4	20
B (17.2-20)	61	81	162	23	39	19	19	0	19	123	427	0.6	19
C (20.5-23.3)	94	94	183	60	6	0	6	-6	6	160	497	0.4	11

Figure 2. Metabolic network and carbon flux distributions, based on ^{13}C labeling experiments with the Sensor reactor system, during the L-Phe production phase under tyrosine-limited conditions. Monitored are the periods 14−16.75 h (A), 17.2−20 h (B), and 20.5−23.3 h (C). All fluxes are standardized to the corresponding glucose uptake rates thus representing mol %. Reverse fluxes are indicated by a minus sign. Because for ^{13}C flux analysis an lumped PEP/PYR pool was used, the carbon flux from PEP to PYR was reconstructed solely on the basis of stoichiometric constraints leading to a flux portion for *pts*-based PEP conversion (left box) and the resulting net flux catalyzed by phosphoenolpyruvate synthase and pyruvate kinase (right box). The optimal flux distribution for L-Phe production (**Opt**) was calculated for nongrowing cells. It is assumed that sufficient transhydrogenase activity enables the nonlimited convertion of NADH into NADPH and vice versa. ATP is gained by respiration (1.8 ATP/NADH). The reaction names are given in analogy to the model (Table 5).

statistically identifiable. This observation needs to be stressed because it illustrates the potential drawback of a single metabolic flux analysis, which, by retrospective analysis, could reveal the insufficiency of the experimental data measured during the prechosen observation window. If a serial flux analysis is carried out as presented below, potential data limitations could be overcome, additionally uncovering systematic flux changes, which were not accessible with a single snapshot study.

Studying the current results from 14 to 23.3 h process time, the series of flux maps allows the conclusion that a continuously increasing fraction of carbon was metabolized via glycolysis (*emp1*) compared to the branching off into the oxidative pentose phosphate pathway (*ppp1*). As a consequence, transketolase (*ppp4*, *ppp5*)- and transaldolase (*ppp6*)-catalyzed fluxes of the pentose-phosphate pathway declined significantly, giving rise to the assumption that the E4P precursor supply for the aromatic amino acid pathway decreased concomitantly. As illustrated in Figure 2, the lumped PEP/PYR pool of ^{13}C analysis was decomposed by stoichiometric analysis, allowing the estimation of a net flux via pyruvate kinase and the inversely directed phosphoenolpyruvate synthase (Pps) reaction. The serial flux analysis indicates that the *pykA* and *pykF* encoded kinase reaction obviously increasingly dominated the net flux and subsequently amplified the flux into the tricarboxylic acid cyclic from 114 to 160 mol %. As a consequence, CO_2 formation steadily increased from 416 to 497 mol %, while at the same time L-Phe formation rates reduced from 20 to 11 mol %. It is noteworthy, that cultivation conditions such as pH, temperature, etc. did not change during this period (see Figure 1). Also, the availability of the sole carbon source glucose as well as the tyrosine supply and oxygen availability were unchanged during the entire observation.

To compare the observed flux distributions with a theoretical flux map describing an optimum L-Phe production yield, the tabulated data in Figure 2 are given. Most strikingly, an optimum L-Phe formation of 59.7 mol % is calculated providing that the tricarboxylic acid cycle was inactive in nongrowing cells. As a consequence, the

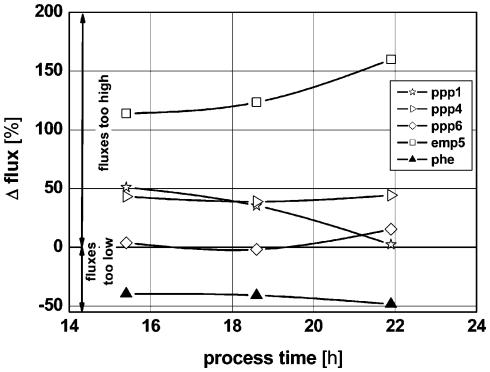

Figure 3. Flux difference Δ is calculated as the difference between the experimentally determined flux [mol % of glucose uptake] during the production phase and the corresponding flux at optimum carbon flux distribution as shown in Figure 2. Flux maps refer to the half-time of each labeling period. For flux abbreviations, see Figure 2 and Table 5.

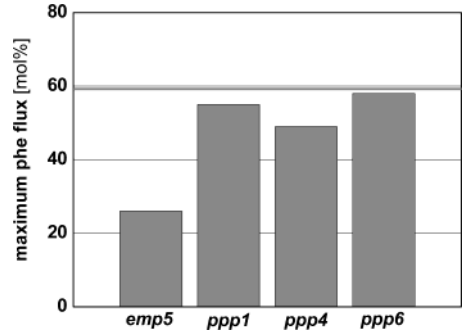

Figure 4. Maximum achievable L-Phe flux [mol %] based on the assumption that one observed flux (*emp5*, *ppp1*, *ppp4*, or *ppp6* of phase A) could not be modified. The glucose uptake was kept constant (*upt* = 1), and the rest of the metabolic network could reroute carbon fluxes such that a maximum L-Phe formation is achieved. The straight line indicates the upper 59.7 mol % L-Phe optimum, which is reachable according to the linear programming results presented in Figure 2.

pts-caused PYR formation is redirected into PEP via Pps (−100 mol %). Interestingly, only a small flux of 3.3 mol % via the oxidative pentose-phosphate route is favored compared to a significant transketolase activity (*ppp4*) providing a high flux of −38.7 mol % into the E4P pool. Together with the incoming transaldolase reaction (*ppp6*), 59.7 mol % of E4P is thus delivered into the aromatic amino acid pathway. Interestingly, under optimum L-Phe production conditions, a reaction cycle is built up taking GAP and F6P from glycolysis and transferring them into E4P and X5P; the latter is subsequently converted into Ru5P and further metabolized via *ppp3* into Ri5P and then back into GAP. This demonstrates that all pentose-phosphate reactions must be well equilibrated to enable an optimum E4P supply, including transketolase and transaldolase as well as the phosphoribose isomerase (*ppp3*) and the ribulose 5-phosphate 3-epimerase (*ppp2*).

Figure 3 gives an overview of the differences between measured and theoretical fluxes considering the most important reactions of glycolysis, the pentose-phosphate pathway, and the aromatic amino acid pathway. Even at the beginning of the production phase, which was previously identified as the best production period, the flux distribution was far from optimal. The flux via oxidative pentose phosphate pathway (*ppp1*) was about 50 mol % too high. Similar observations were made for the transketolase reaction *ppp4*, and an even worse situation was found for the net flux via PykA/PykF and Pps (*emp5*). Against it, the transaldolase reaction *ppp6* showed an almost optimum flux and kept this level, although the measured L-Phe/glucose yield achieved only 20%, compared to the theoretical value of 59.7%. From this, we concluded that transaldolase is probably not the most interesting metabolic engineering target. This statement partly contradicts previous findings of Lu and Liao (1997) who identified a positive effect of *tal* overexpression for DAHP production. However, no amplified DAHP synthase was used in their study and DAHP production was investigated with partly growing cells in shaking flask cultures, which significantly differed from the experimental conditions of Sensor reactor experiments.

Figure 3 reveals that large differences occurred between (theoretical) optimal and measured fluxes for transketolase (*ppp4*) and the net reaction of PykA/PykF and Pps (*emp5*). The flux differences coincided with low (insufficient) L-Phe/glucose yields, which even deteriorated during the course of observation. The findings are in agreement with previous studies of Draths et al. (1992) and Li et al., (1999), emphasizing the necessity of *tktA* overexpression. Our observations also support the results of Patnaik and Liao (1994), Patnaik et al. (1995), Berry (1996), Gosset (1996), Yi et al. (2002), and Chandram et al., (2003), who stressed the common overexpression of *tktA* and *pps* to achieve an increased flux into aromatic amino acid synthesis.

On the basis of the metabolic flux analysis presented so far, the additional aim was followed to qualify the observed flux deviations from the optimum such that the identification of the most interesting metabolic engineering target was possible. Therefore, flux sensitivity analysis was performed as described in the previous section. As an example, the results of the best L-Phe production phase (phase A) are presented in Figure 4. It is clearly identifiable that *emp5*, coding for the net reaction of PykA/PykF and Pps, represents the reaction that mostly limited the maximum achievable L-Phe formation. In the case of transaldolase (*ppp6*), its low limiting impact on the L-Phe formation became obvious, because the theoretical optimum of 59.7 mol % was almost achievable with a fixed *ppp6* flux. Fixing the transketolase reaction, encoded by *ppp4*, still afforded 49 mol % L-Phe flux. Hence, *emp5* should be the preferred metabolic engineering target to improve the existing L-Phe production strain.

However, the identification of *emp5* (see Figures 3 and 4) as a promising metabolic engineering target as such is not sufficiently unequivocal, because *emp5* codes for the net flux of PykA/PykF and the conversely directed Pps reaction. Furthermore, the question should be addressed of why this flux even deteriorated, showing increasing net fluxes during the observed phases (see Figures 2 and 3). Therefore, a working hypothesis is derived taking into account that increasing net fluxes indicate rising PykA/PykF rates together with decreasing Pps rates.

In the case of PykA/PykF, FBP (and to a minor extent G6P and Ri5P) activates the kinase activity (Valle et al., 1996). Provided that increasing glycolytic fluxes (see absolute flux values in Table 1) also entailed increasing FBP pool sizes because of underlying Michelis−Menten-type reaction kinetics, an increase in pyruvate kinase activity would be the consequence. Furthermore, Pps activity can be inhibited by *tca* metabolites such as 2-oxoglutarate (AKG) and oxaloacetate (OAA; Cooper and Kornberg, 1974; Chulavatnatol and Atkinson, 1973), both important precursors for amino acid synthesis, which was not active in the nongrowing *E. coli* cells of this study.

Regarding the increased, absolute *tca* fluxes and following the same argumentation as above, a diminished Pps activity would be the consequence.

Hence, deteriorating L-Phe/glucose levels could be caused by decreasing Pps activity together with increasing PykA/PykF activity, both regulated on a biochemical level by enzyme inhibition and/or activation, respectively. *pps* overexpression could thus be an appropriate means to compensate a potential Pps inhibition and to redirect the PykA/PykF flux. However, total flux redirection from PYR to PEP (as proposed by linear optimization) could only be achieved if *pykA* and *pykF* would be completely inactivated in resting cells.

Summary

Compared to the previously estimated maximum DAHP/glucose yield of 86 mol % (Patnaik et al., 1995), these linear programming studies estimate maximum L-Phe/glucose yields of about 60 mol %, which is clearly a consequence of the additional PEP needed for L-Phe synthesis. While early works with DAHP-producing strains succeeded to convert glucose to DAHP with (almost) theoretical yields (Liao et al., 1996), our flux analysis results show that the L-Phe producing *E. coli* strain only reaches a third of the maximum L-Phe/glucose yield during the L-tyrosine-limited production period. Therefore, the Sensor reactor was applied in three subsequent observation periods from 14 to 23.3 h process time to elucidate whether and how the resulting serial flux patterns give rise to the identification of metabolic engineering targets for further strain improvement.

Most strikingly, it was found that the observed carbon flux distributions were far from an optimal flux pattern with respect to L-Phe production (at all times), especially because the net flux via PykA/PykF and Pps steadily increased, which entailed reducing L-Phe formation rates from 20 to 11 mol %.

Thanks to the time-variant flux analysis patterns observed, it was thus possible to formulate working hypotheses considering the basic characteristics of the enzyme kinetics involved. Hence, the maybe unexpected hypothesis is formulated that increasingly high intracellular oxaloacetate and 2-oxoglutarate levels presumably cause Pps inhibition, which coincides with PykA/PykF activation due to increased FBP levels. Hence, *pps* overexpression in combination with (at least partly) inactivation of *pykA* and/or *pykF* would be a promising way to optimize L-Phe formation in the current production strain. However, to validate this working hypothesis, detailed measurements of in vivo metabolite concentrations have to be performed, thus leading to a concerted approach of serial metabolic flux analysis and metabolic profiling studies in the future.

Notation

AcCoA	acetyl-CoA
AKG	α-keto glutarate, 2-oxoglutarate
CTR	carbon dioxide transfer rate
DAHP	3-desoxy-arabino-heptulosonate-7-phosphate
DHS	3-dehydro shikimic acid
E4P	D-erythrose 4-phosphate
F6P	fructose-5-phosphate
FBP	fructose-1,6-diphosphate
G6P	glucose 6-phosphate
GAP	glycerinaldehyde-3-phosphate
Gluc13C	1-^{13}C-labeled glucose
GlucNat	natively labeled glucose
ICIT	*iso*-citrate
MAL	malate
OAA	oxaloacetate
OUR	oxygen uptake rate
PEP	phosphoenolpyruvate
Pps	phosphoenolpyruvate synthase
pts	phosphoenolpyruvate transfer system
PykA/PykF	pyruvate kinase A, pyruvate kinase F
PYR	pyruvate
Ri5P	ribose-5-phosphate
Ru5P	ribulose-5-phophate
S7P	sedoheptulose-7-phosphate
SHI	shikimic acid
SUC	succinate
tal	gene, coding for transaldolase
TCA	tricarboxylic acid cycle
tkt	gene, coding for transketolase
X5P	xylose-5-phosphate

Acknowledgment

The authors would like to thank Prof. Wandrey for his generous support and the excellent working conditions provided in the Institute of Biotechnology at Forschungszentrum Jülich GmbH. Thanks are also due to Prof. G. Sprenger, University of Stuttgart, Germany, and the team at DSM Biotech GmbH, Jülich (Germany) for their fruitful cooperation in the "FAME" project (BMBF, Grant 0311644), which represented the notional frame of the results presented here. The project was funded by the "Deutsche Forschungsgemeinschaft DFG" TA 241/2-1,2,3 and WI 1705/4-1,2,3.

References and Notes

(1) Berry, A. Improving Production of Aromatic Compounds in *Escherichia coli* by Metabolic Engineering. *TIBTECH* **1996**, *14*, 250−256.

(2) Bongaerts, J.; Krämer, M.; Müller, U.; Raeven, L.; Wubbolts, M. Metabolic Engineering for Microbial Production of Aromatic Amino Acids and Derived Compounds. *Metab. Eng.* **2001**, *3*, 289−300.

(3) Chandram, S. S.; Yi, J.; Draths, K. M.; von Daeniken, R.; Weber, W.; Frost, J. W. Phosphoenolpyruvate Availability and the Biosynthesis of Shikimic Acid. *Biotechnol. Prog.* **2004**, in press.

(4) Chen, R.; Yap, W. M. G. J.; Postma, P. W.; Bailey, J. E. Comparative Studies of *Escherichia coli* Strains Using Different Glucose Uptake Systems: Metabolism and Energetic. *Biotechnol. Bioeng.* **1997**, *56* (5), 583−590.

(5) Chulavatnatol, M.; Atkinson, D. E. Phosphoenolpyruvate Synthetase from *Escherichia coli*. *J. Biol. Chem.* **1973**, *248* (8), 2712−2715.

(6) Cooper, R. A.; Kromberg, H. L. In *The Enzymes*, 3rd ed.; Boyer, P. D., Ed.; 1974; Vol. 16, 631−649.

(7) Delgado, J.; Liao, J. C. Inverse Flux Analysis for Reduction of Acetate Excretion in *Escherichia coli*. *Biotechnol. Prog.* **1997**, *13*, 361−367.

(8) Draths, K. M.; Pompliano, D. L.; Conley, D. L.; Frost, J. W.; Berry, A.; Disbrow, G. L.; Staversky, R. J.; Lievense, J. C. Biocatalytic Synthesis of Aromatics drom D-Glucose: The Role of Transketolase. *J. Am. Chem. Soc.* **1992**, *114*, 3956−3962.

(9) Drauz, K. H.; Hoppe, B.; Kleemann, A.; Krimmer, H.-P.; Leuchternberger, W.; Weckbecker, C. Amino Acids. In *Ullmann's Encyclopedia of Industrial Chemistry*, 5th Completely Revised ed.; Gerhartz, W., Yamamoto, Y. S., Campbell, Th., Pfefferkorn, R., Rounsaville, J. F., Eds.; 2002; Vol. A2.

(10) Drysch, A.; El Massaoudi, M.; Mack, C.; Takors, R.; de Graaf, A. A.; Sahm, H. Production Process Monitoring by Serial Mapping of Microbial Carbon Flux Distributions Using a Novel Sensor Reactor Approach: II − ^{13}C Labelling-Based

Metabolic Flux Analysis and L-Lysine Production. *Metab. Eng.* **2003a**, *5*, 96−107.
(11) Drysch, A.; El Massaoudi, M.; Wiechert, W.; de Graaf, A. A.; Takors, R. Serial Flux Mapping of *Corynebacterium glutamicum* during Fed-Batch L-Lysine Production Using the Senor Reactor Approach. *Biotechnol. Bioeng.* **2004**, *85* (5), 497−505.
(12) El Massaoudi, M.; Spelthahn, J.; Drysch, A.; de Graaf, A. A.; Takors, R. Production Process Monitoring by Serial Mapping of Microbial Carbon Flux Distributions Using a Novel Sensor Reactor Approach: I − Sensor Reactor System. *Metab. Eng.* **2003**, *5*, 86−95.
(13) Ferenci, T. Adaption to Life at Micromolecular Nutrient Levels: The Regulation of *Escherichia coli* Glucose Transport by Endoinduction and cAMP. *FEMS Microbiol. Rev.* **1996**, *18*, 301−317.
(14) Fischer, E.; Sauer, U. Metabolic Flux Profiling of *Escherichia coli* Mutants in Central Carbon Metabolism Using GC-MS. *Eur. J. Biochem.* **2003**, *270* (5), 880−891.
(15) Flores, N.; Xiao, J.; Berry, A.; Bolivar, F.; Valle, F. Pathway Engineering for the Production of Aromatic Compounds in *Escherichia coli*. *Nature Biotechnol.* **1996**, *14*, 620−623.
(16) Flores, S.; Gosset, N.; Flores, N.; de Graaf, A. A.; Bolivar, F. Analysis of Carbon Metabolism in *Escherichia coli* Strains with an Inactive Phosphotransferase System by ^{13}C Labelling and NMR Spectroscopy. *Metab. Eng.* **2002**, *4* (2), 124−137.
(17) Franke, D.; Lorbach, V.; Esser, S.; Dose, C.; Sprenger, G. A.; Halfar, M.; Thömmes, J.; Müller, R.; Takors, R.; Müller, M. (*S*,*S*)-2,3-Dihydroxy-2,3-dihydroxybenzoic Acid: Microbial Access with Engineered Cells of *Escherichia coli* and Applicability as Starting Material in Natural-Product Synthesis. *Chem.—Eur. J.* **2003a**, *9*, 2−10.
(18) Franke, D.; Sprenger, G. A.; Müller, M. Easy Access to (*R*,*R*)-3,4-Dihydroxy-3,4-dihydrobenzoic Acid with Engineered Strains of *Escherichia coli*. *Chem. Biol. Chem.* **2003b**, *4*, 775−777.
(19) Frost, J. W.; Lievense, J. Prospects for Biocatalytic Synthesis of Aromatics in the 21st Century. *New J. Chem.* **1994**, *18*, 341−348.
(20) Gerigk, M. R.; Maass, D.; Kreutzer, A.; Sprenger, G.; Bongaerts, J.; Wubbolts, M.; Takors, R. Enhanced Pilot-Scale Fed-Batch L-Phenylalanine Production with Recombinant *Escherichia coli* by Fully Integrated Reactive Extraction. *Bioproc. Biosyst. Eng.* **2002**, *25*, 43−52.
(21) Gosset, G.; Yong-Xiao, J.; Berry, A. A Direct Comparison of Approaches for Increasing Carbon Flow to Aromatic Biosynthesis in *Escherichia coli*. *J. Indust. Microbiol.* **1996**, *17*, 47−52.
(22) Li, K.; Mikola, M. R.; Draths, K. M.; Worden, R. M.; Frost, J. W. Fed-Batch Fermentor Synthesis of 3-Dehydroshikimic Acid Using Recombinant *Escherichia coli*. *Biotechnol. Bioeng.* **1999**, *64* (1), 61−73.
(23) Liao, J. C.; Hou, S. Y.; Chao, Y. P. Pathway Analysis, Engineering, and Physiological Consideration for Redirecting Central Metabolism. *Biotechnol. Bioeng.* **1996**, *52*, 129−140.
(24) Lu, J.-L.; Liao, J. C. Metabolic Engineering and Control Analysis for Production of Aromatics: Role of Transaldolase. *Biotechnol. Bioeng.* **1997**, *53* (2), 132−138.
(25) Möllney, M.; Wiechert, W.; Kowantzki, D.; de Graaf, A. A. Bidirectional Reaction Steps in Metabolic Networks. IV. Optimal Design of Isotopomer Labeling Experiments. *Biotechnol. Bioeng.* **1999**, *66*, 86−103.
(26) Ogden, G.; Földi, P. 1992 Amino Acid Analysis: An Overview of Current Methods. *LC-GC Int.* 5/1, 28−39.
(27) Patnaik, R.; Liao, J. C. Engineering of *Escherichia coli* Central Metabolism for Aromatic Metabolite Production with Near Theoretical Yield. *Appl. Environ. Microbiol.* **1994**, *10*, 3903−3908.
(28) Patnaik, R.; Spitzer, R. G.; Liao, J. C. Pathway Engineering for Production of Aromatics in *Escherichia coli*: Confirmation of Stoichiometric Analysis by Independent Modulation of AroG, TktA, and Pps Activities. *Biotechnol. Bioeng.* **1995**, *46*, 361−370.
(29) Peekhaus, N.; Conway, T. What is for Dinner?: Entner−Doudoroff Metabolism in *Escherichia coli*. *J. Bacteriol.* **1998**, *180* (14), 3495−3502.
(30) Rüffer, N.; Heidersdorf, U.; Kretzers, I.; Sprenger, G. A.; Raeven, L.; Takors, R. Fed-Batch L-Phenylalanine Production with Recombinant *E. coli* Using Liquid−Liquid Centrifuges for Integrated Product Separation and Concentration, **2004**, *Bioproc. Biosys. Eng.*, accepted.
(31) Schmid, A.; Dordick, J. S.; Hauer, B.; Kiener, A.; Wubbolts, M.; Witholt, B. Industrial Biocatalysis Today and Tomorrow. *Nature* **2001**, *409*, 258−268.
(32) Tatarko, M.; Romeo, T. Disruption of a Global Regulators Gene to Enhance Central Carbon Flux into Phenylalanine Biosynthesis in *Escherichia coli*. *Curr. Microbiol.* **2001**, *43* 26−32.
(33) Valle, F.; Munoz, E.; Ponce, E.; Flores, N.; Boliar, F. Basic and Applied Aspects of Metabolic Diversity: The Phosphoenolpyruvate Node. *J. Ind. Microbiol.* **1996**, *17*, 458−462.
(34) Wiechert, W.; Möllney, M.; Isermann, N.; Wurzel, M.; de Graaf, A. A. Bidirectional Reaction Steps in Metabolic Networks. III. Explicit Solution and Analysis of Isotopomer Labeling Systems. *Biotechnol. Bioeng.* **1999**, *66*, 69−85.
(35) Yi, J.; Li, K.; Draths, K. M.; Frost, J. W. Modulation of Phosphoenolpyruvate Synthase Expression Increases Shikimate Pathway Product Yields in *E. coli*. *Biotechnol. Prog.* **2002**, *18*, 1141−1148.
(36) Zeppenfeld, T.; Larisch, C.; Lengeler, J. W.; Jahreis, K. Glucose Transporter Mutants of *Escherichia coli* K-12 with Changes in Substrate Recognition of IICB(Glc) and Induction Behavior of the ptsG gene. *J. Bacteriol.* **2000**, *182*, 4443−4452.

Accepted for publication January 26, 2004.

BP0342755